Solving Controversies on the Iron Phase Diagram Under High Pressure

Morard, Guillaume; Boccato, Silvia; Rosa, Angelika D.; Anzellini, Simone; Miozzi, Francesca; Henry, Laura; Garbarino, Gaston; Mezouar, Mohamed; Harmand, Marion; Guyot, François

Total number of authors:
14

Published in:
Geophysical Research Letters

Link to article, DOI:
10.1029/2018GL079950

Publication date:
2018

Document Version
Publisher's PDF, also known as Version of record

Geophysical Research Letters

RESEARCH LETTER
10.1029/2018GL079950

Key Points:
- Melting curve and phase diagram of pure Fe has been measured by in situ X-ray absorption up to 130 GPa
- Overall agreement between different in situ studies leads to a melting temperature of 4250 ± 250 K at core-mantle boundary pressure
- Discrepancies with previous measurements is unambiguously attributed to carbon contamination from the diamonds or thermal pressure overestimation

Supporting Information:
- Supporting Information S1

Correspondence to:
G. Morard,
guillaume.morard@upmc.fr

Citation:
Morard, G., Boccato, S., Rosa, A. D., Anzellini, S., Miozzi, F., Henry, L., et al. (2018). Solving controversies on the iron phase diagram under high pressure. *Geophysical Research Letters*, *45*, 11,074–11,082. https://doi.org/10.1029/2018GL079950

Received 7 AUG 2018
Accepted 8 OCT 2018
Accepted article online 12 OCT 2018
Published online 25 OCT 2018

Solving Controversies on the Iron Phase Diagram Under High Pressure

Guillaume Morard[1], Silvia Boccato[2], Angelika D. Rosa[2], Simone Anzellini[3], Francesca Miozzi[1], Laura Henry[2], Gaston Garbarino[2], Mohamed Mezouar[2], Marion Harmand[1], François Guyot[1], Eglantine Boulard[1], Innokenty Kantor[2,4], Tetsuo Irifune[5], and Raffaella Torchio[2]

[1]Sorbonne Université, Institut de Minéralogie, de Physique des Matériaux et de Cosmochimie, IMPMC, Museum National d'Histoire Naturelle, UMR CNRS 7590, IRD, Paris, France, [2]European Synchrotron Radiation Facility, Grenoble, France, [3]Diamond Light Source Ltd., Didcot, UK, [4]Institut for Fysik, Danmarks Tekniske Universitet, Kongens Lyngby, Denmark, [5]Geodynamics Research Center, Ehime University, Matsuyama, Japan

Abstract As the main constituent of planetary cores, pure iron phase diagram under high pressure and temperature is of fundamental importance in geophysics and planetary science. However, previously reported iron-melting curves show large discrepancies (up to 1000 K at the Earth's core–mantle boundary, 136 GPa), resulting in persisting high uncertainties on the solid-liquid phase boundary. Here we unambiguously show that the observed differences commonly attributed to the nature of the used melting diagnostic are due to a carbon contamination of the sample as well as pressure overestimation at high temperature. The high melting temperature of pure iron under core-mantle boundary (4250 ± 250 K), here determined by X-ray absorption experiments at the Fe K-edge, indicates that volatile light elements such as sulfur, carbon, or hydrogen are required to lower the crystallization temperature of the Earth's liquid outer core in order to prevent extended melting of the surrounding silicate mantle.

Plain Language Summary Iron is the main constituent of planetary cores; however, there are still large controversies regarding its melting temperature and phase diagram under planetary interior conditions. The present study reconciles different experimental approaches using laser-heated diamond anvil cell with different in situ X-ray diagnostics (absorption, diffraction, and Mossbauer spectroscopy). The main reason of discrepancies (over 1000 K at core-mantle boundary conditions) is attributed to carbon contamination from the diamond anvils and metrology issues related to thermal pressure overestimation. A high-melting temperature for iron at core-mantle boundary pressure would imply the presence of volatile elements in the liquid outer core, such as sulfur, carbon, or hydrogen, in order to lower its crystallization temperature and avoid extended melting of the surrounding silicate mantle.

1. Introduction

Iron represents the main constituent of planetary cores in our solar system. Its physical properties under high pressure and temperature conditions are therefore extremely important to determine the internal structure and dynamics of telluric planets. One of the key parameters of its phase diagram is the melting curve. Its extrapolation up to the inner-outer core boundary conditions can, in fact, provide information about the temperature profile in planetary cores. This information places important constraints on parameters like heat flux to the mantle, convectional mode, and cooling rate, all of which are fundamental to the planets heat budget and dynamics. However, despite intensive experimental and theoretical efforts, a consensus on the melting line of pure iron has not been found during the last decades.

Pioneering work performed in laser-heated diamond anvil cells (LH-DAC) was using laser speckle technique to detect movement on the sample surface as melting diagnostic (Boehler, 1993). This study has been later confirmed by an in situ LH-DAC X-ray Diffraction (XRD) study using the appearance of diffuse scattering as melting criterion (Boehler et al., 2008) and recently confirmed again by in situ X-ray absorption technique in LH-DAC (Aquilanti et al., 2015). Another recent in situ LH-DAC XRD experiment, also using the appearance of diffuse scattering as melting criterion (Anzellini et al., 2013) has obtained a melting line higher by more than 1000 K above 100 GPa with respect to the X-ray absorption spectroscopy (XAS) measurement (Aquilanti et al., 2015), but in a good agreement with shock experiments (Brown & Mcqueen, 1986;

Nguyen & Holmes, 2004) and ab initio calculations (Alfè, 2009; Alfè et al., 2002). Finally, recent LH-DAC Synchrotron Mossbauer Spectroscopy (SMS) experiments (Jackson et al., 2013; Zhang et al., 2015) have determined a melting temperature falling in between the two previous curves.

The persisting discrepancies in the reported results have caused a long-standing debate among the scientists in the last years, in particular, while comparing the adopted in situ techniques. In fact, even if probing the sample under different scales of resolution of the atomic arrangement (XAS, SMS, and XRD), these techniques should provide the same results within the experimental errors. However, while performing a LH-DAC experiment, several aspects must be considered together with the melting diagnostic to obtain reliable data, which include the sample configuration, possible chemical reactions, and the adopted metrology (see Mezouar et al., 2017). Furthermore, an accurate pressure and temperature evaluation at simultaneous high P/T conditions together with a critical assessment of their errors is essential to provide a reliable measure of the melting line.

In the present study, with the purpose of performing a critical comparison between different melting diagnostics, the melting line of pure Fe has been investigated in situ in LH-DAC by energy dispersed XAS. This is a probe similar to the one employed in Aquilanti et al. (2015). The sample geometry of this study is identical to the one adopted in Jackson et al. (2013) and in Anzellini et al. (2013) but strongly different than the one used in Aquilanti et al. (2015); where the iron sample is contained in a cavity drilled by focused ion beam (FIB) technique in Al_2O_3 single crystals). In addition, a critical analysis of the metrology has been performed during the experiment in order to establish realistic error bars. Finally, an ex situ analysis of the recovered samples has been performed by XRD and SEM techniques to evaluate the presence of chemical reactions and to validate the adopted melting criterion.

The obtained results reveal the different origins of discrepancies between previous studies therefore placing higher constrains on the iron melting line. We show that low melting line is related to carbon contamination and difference in the pressure determination at high temperature. Moreover, the present study provides a refined iron phase diagram up to core-mantle boundary (CMB) pressure, allowing a better evaluation of the amount of light elements present in the core.

2. Materials and Methods

2.1. Experimental Procedure

Laser-heating diamond anvil cell experiments were performed on the energy dispersive X-ray absorption beamline ID24 at the European Synchrotron Radiation Facility, Grenoble (Pascarelli et al., 2016). A highly focused X-ray beam was employed (down to 3*3 μm^2 full width at half maximum) covering an energy range of more than 800 eV (i.e., from 7,000 to 7,800 eV). Two Nd:YAG lasers are focused on the sample using two separate planoconvex lenses with a focal distance of 50 mm, to obtain a laser hotspot on the sample of 15–20 μm of diameter. Detailed description of the laser-heating experimental setup available on ID24 beamline is detailed in Kantor et al. (2018).

Membrane-driven LeToullec-type diamond anvil cells were used to pressurize the sample equipped with either single-crystal or sintered nanopolycrystalline diamonds (Ishimatsu et al., 2012), having culet sizes ranging from flat 300 to beveled 300/150 μm. The latter allowed acquiring glitch-free XAS data over the entire energy range accessible at ID24. The sample consists of a 5-μm thick Fe foil (99.99% purity, GoodFellow), providing an optimized absorption jump. The employment of such thin samples further minimizes axial temperature gradients during laser heating. For all experiments, the Fe foil was sandwiched between two disks of KCl. These disks were prepared by compressing KCl powder to the target thickness (Sigma Aldrich, 99.99% purity). Single disks were then laser-cut using the femto-laser micromachining facility available at Institut de Minéralogie, de Physique des Matériaux et de Cosmochimie laboratory. The employment of pre-compressed KCl disks ensures a controlled and homogeneous insulation thickness, which is a prerequisite for generating a homogenous laser-heating spot reducing the temperature gradients seen by the X-rays. The disks further allowed performing reproducible and fast loadings. In order to limit and remove any contamination of moisture from air, the loading of the pressure medium and the sample were performed within 1 hr, and the loaded DAC was kept open in a vacuum oven at 120 °C for more than 12 hr before pressurizing.

The temperature on the sample was gradually increased by adjusting the laser output power carefully stepwise every 0.1%. The temperature was measured with 1 to 0.01 s exposure time. The typical laser heating

duration is 1.2 s, with a delay of 100 ms before starting the temperature measurement. XAS data were simultaneously acquired by accumulating 10 spectra with 100 ms exposure time. After each temperature step, a spectrum of the quenched sample was acquired to verify that the sample did not react. Details about the data acquisition procedure can be found in Boccato et al. (2017).

The absence of reaction products such as Fe_3C was verified in all recovered samples by acquiring finely meshed (5-μm step size) 2-D XRD maps at the diffraction beamline ID27 using a highly focused X-ray beam of $3 \times 3\ \mu m^2$ ($\lambda = 0.3738$ Å; Mezouar et al., 2005). Diffraction images were integrated with Dioptas (Prescher & Prakapenka, 2015). The Fe_3C phase could be identified in few samples through the presence of single-diffraction spots of the most intense peaks of Fe_3C, that is, (102) at 2.068 Å.

Recovered samples were cut through the hotspot area to analyze the texture using the analysis platform available at Institut de Minéralogie, de Physique des Matériaux et de Cosmochimie. The developed technique combines femtosecond-pulsed laser machining, ion polishing, and FIB cutting, to remove the sample from the gasket and expose the laser-heated area, in order to perform accurate SEM imaging. Extended description of sample preparation can be found in Morard et al. (2017).

2.2. Thermal Pressure Calculation

The pressure was determined at room temperature before and after each heating cycle using either the Raman peak position of the single-crystalline diamond measured at the center of the culet (Akahama & Kawamura, 2004) or using the position of the fluorescence line of a ruby sphere placed in the sample chamber (Dewaele et al., 2008). The sample pressure during laser heating was then calculated following the procedure established in Lord, Wood, et al. (2014) and the equation

$$P = P_{\text{before}} + \frac{P_{\text{after}} + \Delta P - P_{\text{before}}}{T_{\text{max}} - 300} \times (T - 300),$$

where P_{before} and P_{after} are the different pressures measured before and after the heating cycle, T_{max} is the maximal temperature of the heating cycle, and ΔP is the pressure difference between the pressure at high temperature and the pressure measured after the heating cycle. This pressure difference is kept constant for the pressure–temperature range investigated in the present study and fixed at 2 GPa, as highlighted in a recent XRD experiment (Miozzi et al., 2018; see supporting information, and references therein for more details; Campbell et al., 2009; Lord, Wann, et al., 2014). It should be noticed that this equation is only valid for T_{max} superior to 2000 K, as the observed scattering of ΔP (2 ± 1.5 GPa, Figure S4) does not allow us assigning a dependence of ΔP over pressure or temperature.

3. Results

Solid-solid and solid-liquid phase transitions in iron can be unambiguously identified from changes in the X-ray Absorption Near Edge Structure (XANES) region of the absorption spectra at the Fe K-edge (Harmand et al., 2015; Marini et al., 2014; Torchio et al., 2016). In particular, the transition from the high-pressure hcp (hexagonal close-packed) structure to the high-temperature fcc (face centered cubic) structure results in a strong modification of the first XANES oscillation and the appearance of a double feature at 7,130 and 7,140 eV (Figure 1). Similarly, the solid to liquid transition results in marked changes of several XANES features (1) in the preedge regions the shoulder at 7,120 eV disappears and (2) the first XANES oscillation flattens. On this last point, it should be noticed that damping of these features related to melting is different from temperature damping of EXAFS oscillations due to Debye-Waller effect. The K-edge XANES of iron mirrors the electronic transition from the 1s to the empty 4p states. The observed smoothening of the XANES features in the liquid phase can be related to a broader distribution of empty 4p states due to the breaking of crystalline long-range order (Mazevet et al., 2014).

In order to confirm the validity of these in situ X-ray diagnostics, analysis of recovered samples were performed using a FIB (Figure 2). The protocol for studying the recovered samples has been detailed in our previous work on iron alloys (Morard et al., 2017). Borders of the solid and the molten portions of the recovered samples exhibit a regular and an irregular shape, respectively, allowing to discriminate between them. In addition, the texture related with solid grains twinning is visible in the solid portion of the sample,

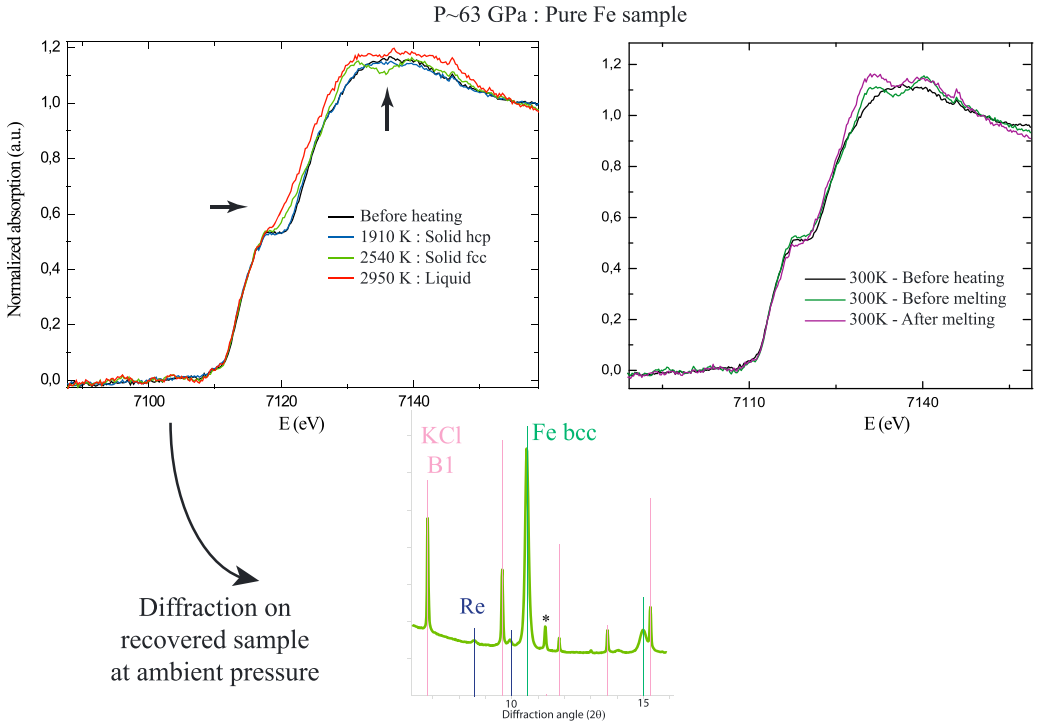

Figure 1. Evolution of X-ray Absorption Near Edge Structure (XANES) spectra at Fe absorption edge upon melting**.** Evolution of XANES spectra from hcp structure (in blue), to fcc structure (in green), and above the melting point (in red). Changes related to the hcp-fcc transition are visible in the edge, with a change from one to two features. Changes related to melting is visible with the disappearance of the feature in the preedge and the flattening in the edge. Arrows indicate these modifications on the XANES signal. Corresponding spectra of quenched sample after each temperature do not show any change in the flank, in agreement with the absence of sample contamination. Diffraction pattern of recovered sample indicates no additional phases, except one peak potentially belonging to the gasket holder (signaled by a star). hcp = hexagonal close-packed; fcc = face centered cubic.

whereas the liquid portion is found to be homogeneous (central portion of the sample on Figures 2 and S5). Thanks to these ex situ analyses we were able to validate the use of the disappearance of the features in the first oscillation and the flattening of the preedge in the XAS spectra, as melting criteria for Fe, similar to our conclusions for the melting of Ni under high pressure (Boccato et al., 2017).

Along with the validation of the in situ melting criterion, a critical examination of the adopted metrology has been performed during the experiment. In particular, each temperature measurement has been analyzed via two-color pyrometry (Benedetti & Loubeyre, 2004), and individual error bars have been assigned (Figure S2). Concerning the pressure measurement, its value under high temperature is estimated considering the thermal contribution. In particular, the value of this thermal pressure strongly depends on the pressure medium compressibility (Lord, Wood, et al., 2014), leading to small value when KCl is used: here a constant value of 2 GPa has been assigned as based on XRD measurements of KCl embedded samples (see section 2 and supporting information). Individual error bars for pressure of ±5 GPa is estimated to summarize the addition of different pressure uncertainties, such as pressure gradient in the sample chamber or uncertainty on the thermal pressure estimation, for example.

Following the previous considerations, the melting points resulting from the SMS study (Jackson et al., 2013; Zhang et al., 2015), who used a sample geometry similar to the present one (Fe foil embedded in KCl), have been revised. In particular, the thermal pressure calculation presented here in the supporting information can be applied to the SMS studies (Jackson et al., 2013; Zhang et al., 2015), resulting in an excellent agreement between their recalculated melting temperatures, our XANES study, and the previous XRD study of Anzellini et al. (2013; Figure 3). The obtained results highlight the fact that these different in situ techniques are all valid, and the previously observed differences arise from uncertainties in the metrology rather than on the adopted melting criteria. Therefore, a revised fit for the different phase boundary is presented to take into

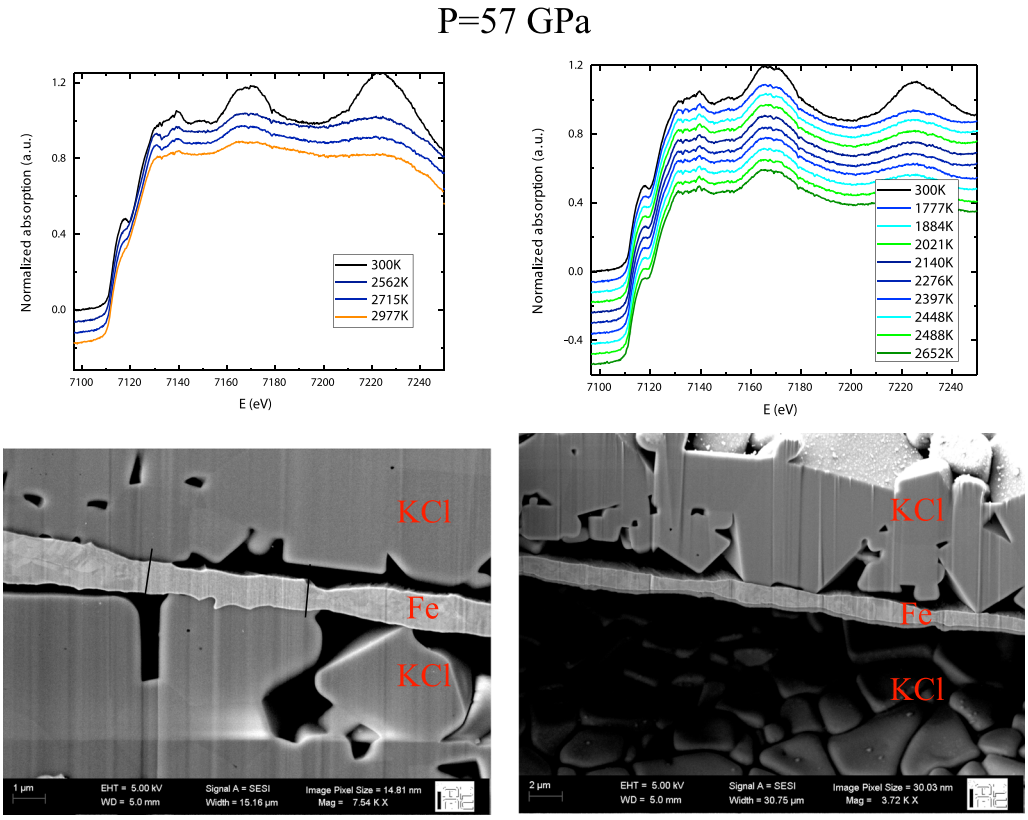

Figure 2. Validation of the melting criteria related to Fe XANES changes. Series of XANES spectra as a function of increasing temperature above (left) and below (right) the melting temperature of Fe. This melting criterion has been validated by focused ion beam cutting and SEM imaging of the hotspot cross section. Changes in the texture and irregular borders due to melting are identified on SEM figure on the left (the black lines delimitate the liquid portion of the sample). Full SEM images with a better resolution are available in the supporting information (Figures S5 and S6). XANES = X-ray Absorption Near Edge Structure; SEM = Scanning Electron Microscope.

account small divergence (below 200 K) between XANES, SMS, and XRD results, especially around the liquid-hcp-fcc triple point (Figure 3 and supporting information; Simon & Glatzel, 1929; Swartzendruber, 1982).

The collected data allowed to bracket the melting curve of iron, between the last solid and the first appearance of the melt (Figure 3 and Table S1). The measurements show an excellent agreement with the melting data from Anzellini et al. (2013) from ambient pressure up to 80 GPa. A small discrepancy can be noticed around 80–100 GPa, where the present study supports a slight bending of the pure Fe melting curve around the hcp-fcc-liquid triple point. A flattening of the melting curve around the triple point can be expected, in relation to change in entropy of melting between the two solid polymorphs. A similar behavior is in fact observed in the case of tin (Barnett et al., 1963). According to our measurements, the triple point of pure Fe is located at 100 ± 10 GPa and 3,500 ± 200 K.

Under higher pressures, our data set follows a similar trend as Anzellini et al. (2013), however, potentially showing higher melting temperature. But significant error bars on these two extreme pressure-melting points (over 500 K) do not allow us to highlight a real divergence between the two studies at the CMB pressure. A melting temperature of 4250 ± 250 K is well representative of the present melting measurements.

In few laser-heating runs of the present study, significantly lower melting temperatures were obtained. Interestingly, these points agree with those reported in previous studies employing the XAS and/or speckle-melting criterion (Aquilanti et al., 2015; Boehler, 1993; Figure 4). For these samples, the melting signature on the Fe XANES is relatively similar to the highest-temperature melting points (Figure 5). However, the signal of the quenched sample between each laser heating clearly highlights an evolution toward the

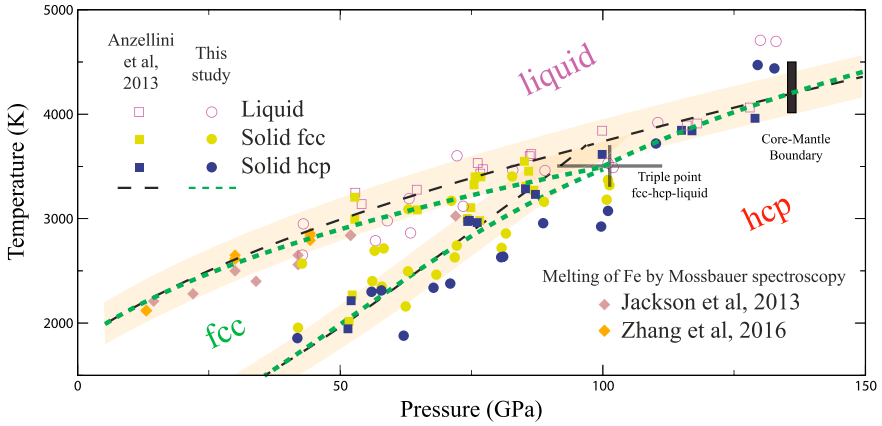

Figure 3. Iron phase diagram combining our X-ray Absorption Near Edge Structure (XANES) data set and previously published Synchrotron Mossbauer Spectroscopy (SMS) and X-ray Diffraction (XRD) data set. Full squares and circles indicate the sample in the solid state for XRD (Anzellini et al., 2013) and XANES experiments respectively. Green color indicates the presence of fcc iron, and blue color indicates the presence of hcp iron. Empty symbols indicate the presence of the first melt. Diamond symbols represent the melting of pure Fe measured by SMS (Jackson et al., 2013; Zhang et al., 2015), with thermal pressure rescaled following the present method (see supporting information for more information). The black dashed line represents the phase diagram boundaries from Anzellini et al. (2013), whereas the green dashed line is adjusted to take into account the three different studies presented here (SMS, XRD, and XANES studies; fitting parameters are available in the supporting information).

disappearance of the preedge signal (Figure 5). We relate the lower melting temperatures to chemical reactions between the sample and the diamond anvils. Indeed, all low melting points are positioned relatively close to the Fe-Fe_3C eutectic melting line (Lord et al., 2009; Morard et al., 2017). In fact, the ex situ XRD analyses of recovered samples with low melting points show clearly the presence of Fe_3C diffraction peaks (Figure 5).

4. Discussion

The present experimental results highlight a convergence between the different experimental techniques used to probe melting in LH-DAC experiments. The melting criterion associated with changes in the

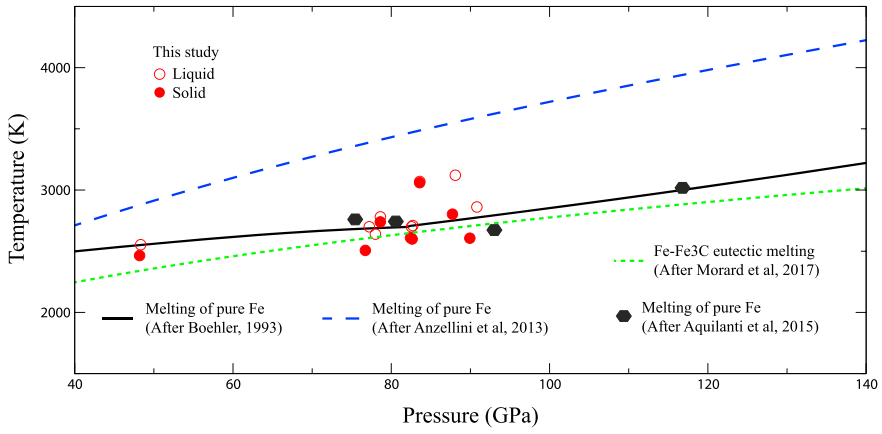

Figure 4. Melting curve of Fe-Fe_3C compared with previous melting of pure Fe measurements and C-contaminated samples from this study. Red circles represent last solid (full symbols) and first liquid (empty symbols) for melting measured by XANES in this study for carbon-contaminated samples (see Figure 5). These measurements are in good agreement with previous melting of Fe determination by speckle (Boehler, 1993) and by XANES (Aquilanti et al., 2015), highlighting that these studies may have determined melting of carbon-contaminated Fe samples. For comparison, the eutectic melting in Fe-Fe_3C system (Morard et al., 2017) is shown as green dashed line and pure Fe melting curve (Anzellini et al., 2013) is shown as blue dashed line. XANES = X-ray Absorption Near Edge Structure.

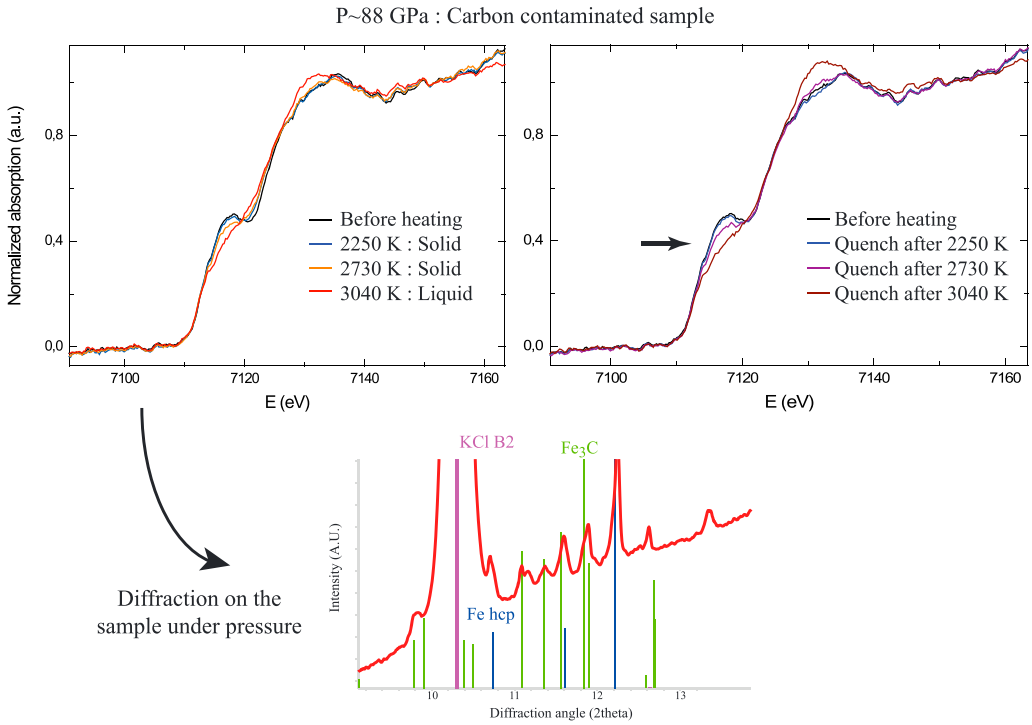

Figure 5. X-ray Absorption Near Edge Structure spectra for carbon-contaminated samples. Melting signature is relatively similar to the one for a pure Fe sample, whereas quench spectra clearly show an evolution related to the carbon enrichment (indicated by an arrow). In addition, diffraction on the sample kept under high pressure clearly shows diffraction peaks of Fe + Fe_3C mixture.

XANES features has been validated through a textural study of the recovered samples from high-pressure laser-heating experiments. Probing the local environment of Fe atoms (XANES and SMS) gives the same melting temperature as probing longer-range structural change evidenced in XRD diffuse scattering appearance. The present critical record of sample reaction after each temperature step and analysis of recovered samples allowed us to evidence that lower-melting temperatures are due to a carbon contamination of Fe sample. This contamination is related to C migration through the pressure medium, reacting with iron in the solid state to form carbides, for example, Fe_3C. This phenomenon has already been discussed in a previous study about carbon transport in LH-DAC (Prakapenka et al., 2003).

We also demonstrate that the thermal pressure determination is an important origin of the observed discrepancies. Estimation of pressure at high temperatures is not straightforward for experiments where XRD signals are not available in situ. In the present study, the thermal pressure is estimated following XRD experiments with similar sample configurations, and it allowed us to reconcile SMS, XRD, and XANES results. We would like to mention the recent attention on the careful comparison between reflective and refractive optics for temperature measurements (Giampaoli et al., 2018; Mezouar et al., 2017). In the present data set an individual error bar is associated to each temperature measurement, using the sliding two-color analysis performed on a large range of wavelengths (from 650 to 900 nm^{-1}; Figure S2). This allows to evaluate the robustness of the temperature for each individual X-ray acquisition.

Combining previous XRD and SMS data set with the present XANES measurements allows to set the position of the triple point hcp-fcc-liquid in the iron phase diagram at 100 ± 10 GPa and 3500 ± 200 K. The location of this specific point is of first importance for the thermodynamic modeling of iron under high pressure (Komabayashi & Fei, 2010). For example, the entropy change upon melting influencing the heat flow at the CMB could be derived from the position of the triple point (Anderson, 1990).

In addition, the melting temperature of pure Fe under CMB pressure is constrained at 4250 ± 250 K. This temperature is close to the solidus temperature of mantle materials (4180 K for peridotitic mantle, Fiquet et al., 2010, and 4150 K for chondritic mantle, Andrault et al., 2011). However, the absence of extended silicate

melting in contact with the metallic liquid outer core at the CMB implies that iron should be alloyed with light elements efficiently lowering its melting temperature. Therefore, volatile elements, such as sulfur, carbon, or hydrogen (Morard et al., 2017; Mori et al., 2016), instead of silicon or oxygen, are required to significantly decrease the temperature of iron crystallization under Earth's core pressure.

5. Conclusions

Combined in situ XANES at Fe edge in LH-DAC and ex situ study of recovered samples by X-ray diffraction and microscopy analysis allowed an unambiguous determination of pure iron-melting curve and phase diagram up to CMB pressure conditions. This data set presents an excellent agreement with previous in situ XRD (Anzellini et al., 2013) and SMS (Jackson et al., 2013), after recalculation of the thermal pressure estimation for the latest one. The triple-point hcp-fcc-liquid in the iron phase diagram is estimated at 100 ± 10 GPa and 3500 ± 200 K and the melting temperature at CMB pressure (136 GPa) at 4250 ± 250 K. This melting temperature, relatively close to the melting temperature of mantle silicates at CMB pressure (Andrault et al., 2011; Fiquet et al., 2010), indicates that volatile light elements such as sulfur, carbon, or hydrogen are required to lower the crystallization temperature of the Earth's liquid outer core and prevent extended melting of the mantle at the contact with the core.

Acknowledgments

Femtosecond laser micromachining at the Institute de Minéralogie de Physique des Matériaux et de Cosmochimie (IMPMC), Paris, has been developed and realized by the "Cellule Project" with the financial support of ANR 2010-JCJC-604-01. Analysis of the recovered samples was performed with the help of I. Estève at the Focused Ion Beam (FIB) and Scanning Electron Microscope (SEM) facility of the Institute de Minéralogie de Physique des Matériaux et de Cosmochimie, supported by Région Ile de France grant SESAME 2006 N°I-07-593/R, INSU-CNRS, INP-CNRS, University Pierre et Marie Curie-Paris 6, and by the French National Research Agency (ANR) grant ANR-07-BLAN-0124-01. This project has received funding from the European Research Council (ERC) under the European Union's Horizon 2020 research and innovation program (grant agreement 670787). Data are available as supporting information.

References

Akahama, Y., & Kawamura, H. (2004). High-pressure Raman spectroscopy of diamond anvils to 250 GPa: Method for pressure determination in the multimegabar pressure range. *Journal of Applied Physics*, *96*(7), 3748–3751. https://doi.org/10.1063/1.1778482

Alfè, D. (2009). Temperature of the inner-core boundary of the Earth: Melting of iron at high pressure from first-principles coexistence simulations. *Physical Review B: Condensed Matter and Materials Physics*, *79*(6), 1–4. https://doi.org/10.1103/PhysRevB.79.060101

Alfè, D., Price, G. D., & Gillan, M. J. (2002). Iron under Earth's core conditions: Liquid-state thermodynamics and high-pressure melting curve from ab initio calculations. *Physical Review B*, *65*(16), 165118. https://doi.org/10.1103/PhysRevB.65.165118

Anderson, O. L. (1990). The high-pressure triple points of iron and their effects on the heat flow from the Earth's core. *Journal of Geophysical Research*, *95*(B13), 21,697–21,707. https://doi.org/10.1029/JB095iB13p21697

Andrault, D., Bolfan-Casanova, N., Lo Nigro, G., Bouhifd, M. A., Garbarino, G., & Mezouar, M. (2011). Solidus and liquidus profiles of chondritic mantle: Implication for melting of the Earth across its history. *Earth and Planetary Science Letters*, *304*(1–2), 251–259. https://doi.org/10.1016/j.epsl.2011.02.006

Anzellini, S., Dewaele, A., Mezouar, M., Loubeyre, P., & Morard, G. (2013). Melting of iron at Earth's inner core boundary based on fast X-ray diffraction. *Science*, *340*(6131). https://doi.org/10.1126/science.1233514

Aquilanti, G., Trapananti, A., Karandikar, A., Kantor, I., Marini, C., Mathon, O., et al. (2015). Melting of iron determined by X-ray absorption spectroscopy to 100 GPa. *Proceedings of the National Academy of Sciences*, *112*(39), 12,042–12,045. https://doi.org/10.1073/pnas.1502363112

Barnett, J. D., Bennion, R. B., & Hall, H. T. (1963). X-ray diffraction studies on tin at high pressure and high temperature. *Science*, *141*, 1041.

Benedetti, L., & Loubeyre, P. (2004). Temperature gradients, wavelength-dependent emissivity, and accuracy of high and very-high temperatures measured in the laser-heated diamond cell. *High Pressure Research*, *24*(4), 423–445. https://doi.org/10.1080/08957950412331331718

Boccato, S., Torchio, R., Kantor, I., Morard, G., Anzellini, S., Giampaoli, R., et al. (2017). The melting curve of nickel up to 100 GPa explored by XAS. *Journal of Geophysical Research: Solid Earth*, *122*, 9921–9930. https://doi.org/10.1002/2017JB014807

Boehler, R. (1993). Temperatures in the Earth's core from melting-point measurements of iron at high static pressures. *Nature*, *363*(6429), 534–536. https://doi.org/10.1038/363534a0

Boehler, R., Santamaría-Pérez, D., Errandonea, D., & Mezouar, M. (2008). Melting, density, and anisotropy of iron at core conditions: New X-ray measurements to 150 GPa. *Journal of Physics: Conference Series*, *121*(PART 2). https://doi.org/10.1088/1742-6596/121/2/022018

Brown, J. M., & Mcqueen, G. (1986). Phase transitions, Griineisen parameter, and elasticity. *Journal of Geophysical Research*, *91*(B7), 7485–7494. https://doi.org/10.1029/JB091iB07p07485

Campbell, A. J., Danielson, L., Righter, K., Seagle, C. T., Wang, Y., & Prakapenka, V. B. (2009). High pressure effects on the iron-iron oxide and nickel-nickel oxide oxygen fugacity buffers. *Earth and Planetary Science Letters*, *286*(3–4), 556–564. https://doi.org/10.1016/j.epsl.2009.07.022

Dewaele, A., Torrent, M., Loubeyre, P., & Mezouar, M. (2008). Compression curves of transition metals in the Mbar range: Experiments and projector augmented-wave calculations. *Physical Review B: Condensed Matter and Materials Physics*, *78*(10), 1–13. https://doi.org/10.1103/PhysRevB.78.104102

Fiquet, G., Auzende, A. L., Siebert, J., Corgne, A., Bureau, H., Ozawa, H., & Garbarino, G. (2010). Melting of peridotite at 140 gigapascals. *Science*, *329*, 1516–1518.

Giampaoli, R., Kantor, I., Mezouar, M., Boccato, S., Rosa, A. D., Torchio, R., et al. (2018). Measurement of temperature in the laser heated diamond anvil cell: Comparison between reflective and refractive Ooptics. *High Pressure Research*, *38*(3). https://doi.org/10.1080/08957959.2018.1480017

Harmand, M., Ravasio, A., Mazevet, S., Bouchet, J., Denoeud, A., Dorchies, F., et al. (2015). X-ray absorption spectroscopy of iron at multi-megabar pressures in laser shock experiments. *Physical Review B: Condensed Matter and Materials Physics*, *92*(2), 1–7. https://doi.org/10.1103/PhysRevB.92.024108

Ishimatsu, N., Matsumoto, K., Maruyama, H., Kawamura, N., Mizumaki, M., Sumiya, H., & Irifune, T. (2012). Glitch-free X-ray absorption spectrum under high pressure obtained using nano-polycrystalline diamond anvils. *Journal of Synchrotron Radiation*, *19*(5), 768–772. https://doi.org/10.1107/S0909049512026088

Jackson, J. M., Sturhahn, W., Lerche, M., Zhao, J., Toellner, T. S., Alp, E. E., et al. (2013). Melting of compressed iron by monitoring atomic dynamics. *Earth and Planetary Science Letters*, *362*, 143–150. https://doi.org/10.1016/j.epsl.2012.11.048

Kantor, I., Marini, C., Mathon, O., & Pascarelli, S. (2018). A laser heating facility for energy-dispersive X-ray absorption spectroscopy. *The Review of Scientific Instruments*, *89*(1), 013,111–013,113. https://doi.org/10.1063/1.5010345

Komabayashi, T., & Fei, Y. (2010). Internally consistent thermodynamic database for iron to the Earth's core conditions. *Journal of Geophysical Research*, *115*, B03202. https://doi.org/10.1029/2009JB006442

Lord, O. T., Walter, M. J., Dasgupta, R., Walker, D., & Clark, S. M. (2009). Melting in the Fe-C system to 70 GPa. *Earth and Planetary Science Letters*, *284*(1–2), 157–167. https://doi.org/10.1016/j.epsl.2009.04.017

Lord, O. T., Wann, E. T. H., Hunt, S. A., Walker, A. M., Santangeli, J., Walter, M. J., et al. (2014). The NiSi melting curve to 70GPa. *Physics of the Earth and Planetary Interiors*, *233*, 13–23. https://doi.org/10.1016/j.pepi.2014.05.005

Lord, O. T., Wood, I. G., Dobson, D. P., Vočadlo, L., Wang, W., Thomson, A. R., et al. (2015). The melting curve of Ni to 1 Mbar. *Earth and Planetary Science Letters*, *408*, 226–236. https://doi.org/10.1016/j.epsl.2014.09.046

Marini, C., Occelli, F., Mathon, O., Torchio, R., Recoules, V., Pascarelli, S., & Loubeyre, P. (2014). A microsecond time resolved X-ray absorption near edge structure synchrotron study of phase transitions in Fe undergoing ramp heating at high pressure. *Journal of Applied Physics*, *115*(9), 093,513–093,515. https://doi.org/10.1063/1.4867619

Mazevet, S., Recoules, V., Bouchet, J., Guyot, F., Harmand, M., Ravasio, A., & Benuzzi-Mounaix, A. (2014). Ab initio calculation of X-ray absorption of iron up to 3 Mbar and 8000 K. *Physical Review B: Condensed Matter and Materials Physics*, *89*(10), 1–5. https://doi.org/10.1103/PhysRevB.89.100103

Mezouar, M., Crichton, W. A., Bauchau, S., Thurel, F., Witsch, H., Torrecillas, F., et al. (2005). Development of a new state-of-the-art beamline optimized for monochromatic single-crystal and powder X-ray diffraction under extreme conditions at the ESRF. *Journal of Synchrotron Radiation*, *12*(5), 659–664. https://doi.org/10.1107/S0909049505023216

Mezouar, M., Giampaoli, R., Garbarino, G., Kantor, I., Dewaele, A., Weck, G., et al. (2017). Methodology for in situ synchrotron X-ray studies in the laser-heated diamond anvil cell. *High Pressure Research*, *37*(2), 170–180. https://doi.org/10.1080/08957959.2017.1306626

Miozzi, F., Morard, G., Antonangeli, D., Clark, A. N., Mezouar, M., Dorn, C., Rozel, A., & Fiquet, G. (2018). Equation of state of SiC at extreme conditions: New insight into the interior of carbon-rich exoplanets. *Journal of Geophysical Research: Planets*, *123*, 2295–2309. https://doi.org/10.1029/2018JE005582

Morard, G., Andrault, D., Antonangeli, D., Nakajima, Y., Auzende, A. L., Boulard, E., et al. (2017). Fe–FeO and Fe–Fe_3C melting relations at Earth's core–mantle boundary conditions: Implications for a volatile-rich or oxygen-rich core. *Earth and Planetary Science Letters*, *473*, 94–103. https://doi.org/10.1016/j.epsl.2017.05.024

Mori, Y., Ozawa, H., Hirose, K., Sinmyo, R., Tateno, S., Morard, G., & Ohishi, Y. (2016). Melting experiments on Fe–Fe_3S system to 254 GPa. *Earth and Planetary Science Letters*, *464*, 135–141. https://doi.org/10.1016/j.epsl.2017.02.021

Nguyen, J. H., & Holmes, N. C. (2004). Melting of iron at the physical conditions of the Earth's core. *Nature*, *427*(6972), 339–342. https://doi.org/10.1038/nature02248

Pascarelli, S., Mathon, O., Mairs, T., Kantor, I., Agostini, G., & Strohm, C. (2016). The time-resolved and extreme-conditions XAS (TEXAS) facility at the European Synchrotron Radiation Facility: The energy-dispersive X-ray absorption spectroscopy beamline ID24. *Journal of Synchrotron Radiation*, *23*(1), 353–368. https://doi.org/10.1107/S160057751501783X

Prakapenka, V., Shen, G., & Dubrovinsky, L. (2003). Carbon transport in diamond anvil cells. *High Pressure High Temperature*, *35/36*, 237–249. https://doi.org/10.1068/htjr098

Prescher, C., & Prakapenka, V. B. (2015). DIOPTAS: A program for reduction of two-dimensional X-ray diffraction data and data exploration. *High Pressure Research*, *35*(3), 223–230. https://doi.org/10.1080/08957959.2015.1059835

Simon, F., & Glatzel, G. (1929). Bernerkungen zur Schmelzdruckkurve. *Zeitschrift für Anorganische und Allgemeine Chemie*, *178*(1), 309–316. https://doi.org/10.1002/zaac.19291780123

Swartzendruber, L. J. (1982). The Fe (iron) system. *Bulletin of Alloy Phase Diagrams*, *3*(2), 161–165. https://doi.org/10.1007/BF02892374

Torchio, R., Occelli, F., Mathon, O., Sollier, A., Lescoute, E., Videau, L., et al. (2016). Probing local and electronic structure in warm dense matter: Single pulse synchrotron X-ray absorption spectroscopy on shocked Fe. *Scientific Reports*, *6*(1), 1–8. https://doi.org/10.1038/srep26402

Zhang, D., Jackson, J. M., Zhao, J., Sturhahn, W., Alp, E. E., Hu, M. Y., et al. (2015). Temperature of Earth's core constrained from melting of Fe and $Fe_{0.9}Ni_{0.1}$ at high pressures. *Earth and Planetary Science Letters*, *447*, 72–83. https://doi.org/10.1016/j.epsl.2016.04.026